ACS APPLIED MATERIALS & INTERFACES

Research Article

www.acsami.org

Sodium Cholate-Templated Blue Light-Emitting Ag Subnanoclusters: *In Vivo* Toxicity and Imaging in Zebrafish Embryos

Shanmugam Chandirasekar,[†] Chandramouli Chandrasekaran,[‡] Thangavel Muthukumarasamyvel,[†] Ganapasam Sudhandiran,[‡] and Nagappan Rajendiran*[,†]

[†]Department of Polymer Science, University of Madras, Guindy Campus, Chennai 600025, Tamil Nadu, India

[‡]Department of Biochemistry, Cell Biology Laboratory, University of Madras, Guindy Campus, Chennai 600025, Tamil Nadu, India

Supporting Information

ABSTRACT: We report a novel green chemical approach for the synthesis of blue light-emitting and water-soluble Ag subnanoclusters, using sodium cholate (NaC) as a template at a concentration higher than the critical micelle concentration (CMC) at room temperature. However, under photochemical irradiation, small anisotropic and spherically shaped Ag nanoparticles (3−11 nm) were obtained upon changing the concentration of NaC from below to above the CMC. The matrix-assisted laser desorption ionization time-of-flight and electrospray ionization mass spectra showed that the cluster sample was composed of Ag_4 and Ag_6. The optical properties of the clusters were studied by UV−visible and luminescence spectroscopy. The lifetime of the synthesized fluorescent Ag nanoclusters (AgNCs) was measured using a time-correlated single-photon counting technique. High-resolution transmission electron microscopy was used to assess the size of clusters and nanoparticles. A protocol for transferring nanoclusters to organic solvents is also described. Toxicity and bioimaging studies of NaC templated AgNCs were conducted using developmental stage zebrafish embryos. From the survival and hatching experiment, no significant toxic effect was observed at AgNC concentrations of up to 200 μL/mL, and the NC-stained embryos exhibited blue fluorescence with high intensity for a long period of time, which shows that AgNCs are more stable in living system.

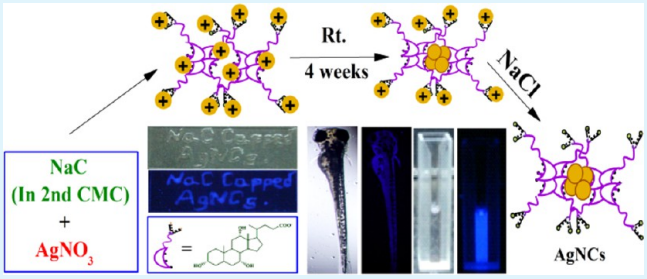

KEYWORDS: *subnanocluster, luminescence, silver, irradiation, zebrafish, imaging*

INTRODUCTION

Subnanometer metal clusters consist of a few to tens of atoms with size <1 nm, which is comparable to the de Broglie wavelength of an electron at the Fermi level (~0.5 nm for Ag and Au).[1,2] In this size regime, the spatial confinement of free electrons results in discrete energy levels, thus leading to interesting molecular-like properties such as a steplike feature in the absorption profile,[3] unusual intrinsic magnetism,[4] and strong size-dependent fluorescence over a wide range from the ultraviolet to near-infrared (NIR) region.[5] Therefore, these clusters could be used for chemical sensing, bioimaging, catalysis, and single-molecule studies.[6−10] Though considerable progress in producing Au clusters with well-defined compositions such as Au_8, Au_{11}, Au_{13}, Au_{15}, Au_{18}, Au_{23}, Au_{25}, Au_{36}, and Au_{38}[2,11] has been made in the past few years, there are only limited reports available for the production of atomically precise Ag clusters, because of their ultrasmall size, which creates many more challenges in synthesis and purification because its surface is more susceptible to oxidation and aggregation, especially in aqueous medium.[8] In the past few years, extensive studies have been conducted on the synthesis of the luminescent Ag subnanoclusters using various templates and ligands such as DNA,[12−16] proteins,[17,18] polymers,[19−25] dendrimers,[26] thiols,[27−34] and peptides.[35,36] Dickson et al. have successfully developed DNA and PAMAM dendrimers templated, photostable, highly fluorescent, and water-soluble Ag nanoclusters (AgNCs) with size-dependent tunable emissions from blue to near-IR regions.[5,8,12,26] Many kinds of polymers, including polyelectrolytes,[21,23] polymer microgels,[19] and polymer hydrogels,[20] have been proven to be effective templates for stabilizing the AgNCs in aqueous medium. The absorption and emission properties of polymer-templated AgNCs after a change in solvent polarity have also been reported.[22,24,25] Atomically monodispersed luminescent thiolated AgNCs with a well-defined size can be prepared by either direct reduction approaches or chemical etching routes.[3,29−31] Most of the monolayer-protected and template-assisted AgNCs emit light at wavelengths ranging from the red to near-infrared region.[12−37] However, very few demonstrations of the synthesis of green and blue light-emitting AgNCs are available because of their ultrasmall size in comparison to that of the red light-emitting AgNCs.[5,17,18,20,29,38,39] Though substantial progress

Received: June 13, 2014
Accepted: December 31, 2014
Published: December 31, 2014

DOI: 10.1021/am507291t
ACS Appl. Mater. Interfaces 2015, 7, 1422−1430

has been achieved in the preparation of AgNCs, several synthetic issues remain in the reported methods, such as larger templates, expensive chemicals, toxic reducing agents, and organic solvents, which may limit the biological applications. Therefore, it would be of great interest to develop a facile and convenient procedure for synthesizing stable, highly luminescent, and biocompatible AgNCs.

Herein, we report a novel green chemical approach for the synthesis of blue light-emitting Ag subnanoclusters using sodium cholate (NaC) as the capping and reducing agent. NaC is a naturally occurring steroidal detergent in mammals that aids in the digestion of fat and lipids.[40] The most prominent features of NaC are its amphiphatic nature, chemically different functional groups, enantiomeric purity, structural rigidity, easy availability, and low cost, making them ideal templates for the preparation of AgNCs. The prepared Ag clusters had an ultrasmall size of <1 nm, consisting of four and six Ag atoms core protected by NaC, were highly luminescent, were stable for a high-salt environment, and had excellent photostability. Recently, noble metal NCs, especially AgNCs and AuNCs, were extensively used as potential fluorescent probes for bioimaging applications; their ultrafine size, high stability under physiological conditions, bright fluorescence, biocompatibility, excellent photostability, and low toxicity make them more promising substituents for organic dyes and semiconductor quantum dots.[8] So far, there have been many reports of *in vitro* toxicity studies and bioimaging using these NCs.[2,8] However, there are only a limited number of reports of *in vivo* studies available. Wu et al. demonstrated ultrasmall NIR-emitting AuNCs for *in vivo* tumor fluorescence imaging using MDA-MB-45 and HeLa tumor xenograft models.[41] Wang and co-workers recently demonstrated *in vivo* self-bioimaging of tumors through *in situ* biosynthesized fluorescent AgNCs and AuNCs.[42,43] Wang et al. reported *in vitro* and *in vivo* tracking of endothelial cells using fluorescent AuNCs as a biocompatiable probe.[44] Zhang et al. reported tumor-targeted imaging *in vitro* and *in vivo* using protein-stabilized Au_{20} NCs as fluorescent probes.[45] In recent years, the zebrafish (*Danio rerio*) was chosen as an emerging important vertebrate model system for the *in vivo* study of the toxicity of metal nanoparticles (MNPs), therapeutic effects of drug molecules, and environmental effects of toxic chemicals because of the close homology between the zebrafish genome and the human genome.[46−49] Furthermore, huge amounts of zebrafish embryos can be generated and developed quite rapidly and synchronously with well-defined developmental stages; transparent embryonic and larval stages facilitate the direct optical observation of the toxic effects of nanoparticles *in vivo*, and the inexpensive maintenance and small size of the larvae allow conservation of space, time, and resources.[46] Zebrafish embryos possess two distinct membranes, i.e., the outer chorion and the inner vitelline membrane, and a viscous fluid present between the two membranes. The chorion possesses pores (0.5−0.7 μm in diameter) that allow the MNPs to pass through the embryo via passive diffusion.[46] There are many reports available for toxicity studies of carbon nanotubes, a graphene-based nanosystem, nickel nanoparticles, copper nanoparticles, silica nanoparticles, AgNPs, and AuNPs using zebrafish embryos as an *in vivo* model.[50−57] Also, several reports of bioimaging studies of zebrafish embryos using different fluorescent probes are available.[58,59] However, to the best of our knowledge, for the first time here we report *in vivo* toxicity and bioimaging studies of sodium cholate-templated AgNCs using zebrafish embryos.

EXPERIMENTAL SECTION

Materials. Silver nitrate (99.99%), sodium cholate (~98%), potassium bromide (99.9%), DCTB {*trans*-2-[3-(4-*tert*-butylphenyl)-2-methyl-2-propenyldidene]malononitrile} (99.9%), and phenylethanethiol (99.99%) were obtained from Sigma-Aldrich. Sodium chloride (99.99%), potassium chloride (99.9%), calcium chloride (99.9%), magnesium sulfate (99%), and toluene (99%) were obtained from Loba-Chemie Ltd. All glassware was thoroughly cleaned with aqua regia (3:1 HCl:HNO_3 ratio), rinsed with doubly distilled water, and dried in an oven prior to being used.

Synthesis of AgNCs. Stock solutions of 4 mM $AgNO_3$, 0.1 M NaCl, and 0.1 M NaC were prepared using deionized doubly distilled water, and the subsequent dilutions were made from this stock solution. For all the experiments, the reaction mixture was maintained at neutral pH. Approximately 0.75 mL of the $AgNO_3$ stock solution was mixed with an aqueous solution of 0.05 M NaC [in a second critical micelle concentration (CMC)] in 25 mL while it was being stirred constantly for 10 min, and the reaction mixture was stored at room temperature in the dark. After 4 weeks, the resulting solution emits intense blue fluorescence under UV light at 365 nm, indicating the formation of Ag subnanoclusters. The unreacted Ag^+ ions present in the cluster solution were removed by filtration in the form of AgCl that was precipitated upon addition of 25 μL of NaCl.

Synthesis of AgNPs. To optimize the reaction conditions, 0.1 mL of the $AgNO_3$ stock solution was added to different concentrations of NaC from below (0.0015 M) to above (0.05 M) the CMC, and the final volume was adjusted to 3 mL using deionized doubly distilled water. The reaction was conducted under UV light irradiation at 365 nm with constant stirring for 7 h. The formation of AgNPs was observed by the gradual change in the color of the solution from colorless to yellow.

Ligand Exchange Reaction. The synthesized AgNCs (5 mL) were mixed with 0.015 M phenylethanethiol in 5 mL of toluene and stirred for 1 h at room temperature. The exchanged clusters from the water to toluene layer were confirmed by the color change observed under UV light at 365 nm. The toluene layer was evaporated and washed with water to remove the excess thiol, and the residue was redissolved in toluene.

Characterization. UV−visible absorption spectra were recorded using a Shimadzu UV-1601 spectrophotometer over the range of 200−1100 nm. The Fourier transform infrared (FT-IR) spectral measurements were taken using a PerkinElmer FT-IR spectrometer. The pressed pellet was prepared by grinding lyophilized NaC-capped AgNP powder with KBr in a 1:100 ratio and analyzed in the spectral range of 4000−400 cm^{-1}. Steady state fluorescence measurements were taken by using a fluorescence spectrophotometer (Fluoromax 4P, Horiba Jobin Yvon). Time-resolved fluorescence decays were obtained by the time-correlated single-photon counting (TCSPC) technique (IBH, model 5000U). The second harmonic output (375 nm) was generated by a flexible harmonic generator (Spectra Physics, GWU 23PS). A vertically polarized 375 nm laser was used to excite the samples. High-resolution transmission electron microscopy (HR-TEM) images were obtained using a FEI-TECHNAI, G2MODEL instrument (T-30 S-TWIN) at an acceleration voltage of 250 kV. The samples were drop cast onto a carbon-coated copper grid and allowed to dry at room temperature before being analyzed. XPS measurements were performed with an Omicron Nanotechnology, GmBH, XM1000 monochromator with Al Kα radiation of 1483 eV operated at 300 W (20 mA emission current, 15 kV) and a base pressure of 5×10^{-5} mbar. The survey scan was performed with a step size of 0.5 eV along with 50 eV as the pass energy. The high-resolution scan was conducted with 0.03 eV as the step size and 20 eV as the pass energy with three sweep segments. The mass spectrometric studies were conducted using a Voyager DE PRO Biospectrometry Workstation (Applied Biosystems) matrix-assisted laser desorption ionization time-of-flight mass spectrometry (MALDI-TOF MS) instrument. A 337 nm pulsed nitrogen laser was used (maximal firing rate of 20 Hz, maximal pulse energy of 300 mJ) for desorption ionization, and TOF was operated in the delayed extraction mode. For the MALDI MS study, the DCTB

DOI: 10.1021/am507291t
ACS Appl. Mater. Interfaces 2015, 7, 1422−1430

Scheme 1. Mechanisms of Formation of NaC-Capped AgNCs and AgNPs and TEM Images of (a) AgNCs and AgNPs (b) above and (c) below the CMC.

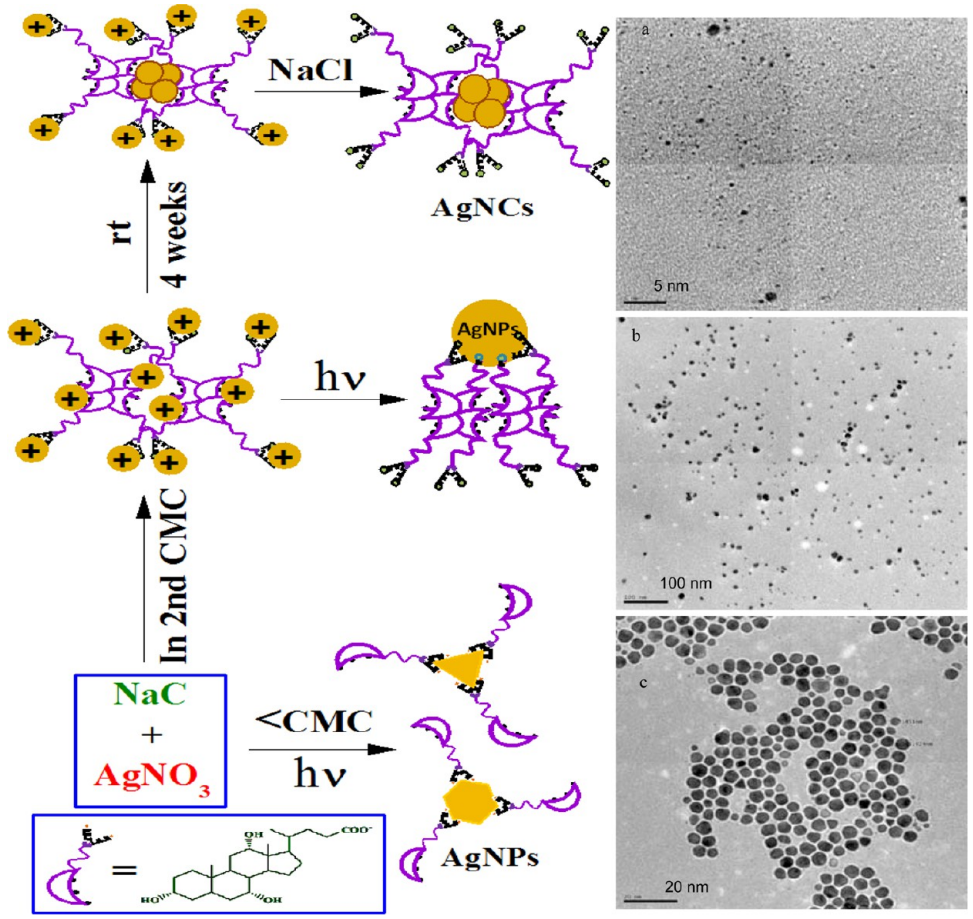

matrix in 50% ethanol (5 mg/mL) and 0.1% trifluoroacetic acid (TFA) was mixed with the silver cluster in water in a 2:1 ratio, sonicated for 1 h, and directly spotted on the target plate. Typical delay times employed were on the order of 75−150 ns. The mass spectra were recorded in positive ion linear mode and averaged for 100 shots. The ESI MS measurements of AgNCs were taken in positive mode using a WATERS-Q-TOF Premier HAB213 instrument in a water/methanol (50:50) solution.

Measurement of the Quantum Yield of AgNCs. The quantum yield of AgNCs was calculated using quinine sulfate (literature quantum yield of 54%) as a reference in 0.1 M H_2SO_4. The emission spectra for the samples were recorded at an excitation wavelength of 366 nm. The quantum yield of AgNCs was determined using eq 1.

$$Q_s = Q_r \times \frac{I_s}{I_r} \times \frac{OD_r}{OD_s} \times \left(\frac{n_s}{n_r}\right)^2 \quad (1)$$

where Q_s and Q_r are the quantum yields of AgNCs and a reference (quinine sulfate), respectively, I_s and I_r are the integrated fluorescence intensities of AgNCs and a reference, respectively, OD_s and OD_r are the optical densities of AgNCs and a reference, respectively, at the excitation wavelength, and n_s and n_r are the refractive indices of AgNCs and a reference solution, respectively.

Toxicity Studies in Zebrafish Embryos. Adult male and female zebrafish (roughly 2:1 male:female sex ratio) were placed in an aquarium that was maintained with controlled light and temperature conditions: 26 °C with a 14 h/10 h light/dark cycle. Spawning was triggered in the morning once the light was turned on. The embryos at 4−5 hpf (hours postfertilization) were collected and washed three times with E3 medium [5 mM NaCl, 0.17 mM KCl, 0.33 mM $CaCl_2$, and 0.33 mM $MgSO_4$ (pH 7.2−7.3)] to remove the surrounding debris prior to imaging. Viable embryos were placed in 24-well culture plates (20 embryos in 2 mL of E3 medium/well). Each group had five replicate wells. The embryos were treated with a dilution series of AgNCs (25, 50, 100, and 200 μL/mL) for 4−96 hpf. The developing embryos in each well were assessed at 4−96 hpf using a bright-field inverted microscope (Motic AE31) attached to a CCD camera, and the numbers of surviving and hatching embryos were recorded at these time points. Fluorescence images of the developing embryos were recorded at late gastrula stage (10 hpf), pharyngula stage (24 hpf), hatching stage (48 hpf), and larval stage (96 hpf) using a dark-field microscope (Olympus IX51) attached to a CCD camera (DP71).

Statistical Analysis. All the statistical analysis was evaluated with SPSS/15 software. Data were analyzed by one-way analysis of variance (ANOVA), and a $p < 0.05$ statistical significance was assumed. The values were expressed as means ± the standard deviation from five independent experiments.

RESULTS AND DISCUSSION

In aqueous solution, NaC exhibits two types of aggregation, i.e., primary (hydrophobic interaction between the NaC molecules) and secondary aggregation (hydrophilic interaction through hydrogen bonding between primary micelles), where the interior of the NaC micelles is more rigid and complex than that of the micelles formed by conventional aliphatic surfactants.[60,61] Upon addition of $AgNO_3$ to the NaC solution (above the CMC), most of the Ag^+ ions bound with COO^- groups were present on the surface of the micelle and a few of them were trapped in the interior of the micelles. At room temperature and neutral pH under dark conditions, the Ag^+

DOI: 10.1021/am507291t
ACS Appl. Mater. Interfaces 2015, 7, 1422−1430

ions present in the interior of the micelles are slowly reduced by -OH groups to form Ag subnanoclusters. Ag^+ ions present on the micellar surface remain unreacted because of the strong electrostatic attraction between COO^- and Ag^+ ions and were removed by filtration in the form of AgCl that was precipitated upon addition of NaCl. However, at basic pH, the Ag^+ ions present in both the interior and on the surface of the micelles are reduced within 24 h, which leads to the formation of larger nanoparticles. However, at acidic pH, the solution exhibited precipitation. The NaC-templated Ag clusters were also stable in the presence of high NaCl concentrations without aggregation, and this could be due to the fact that the clusters are well-protected in the interior of the micelle (Scheme1). The UV−visible spectrum of synthesized Ag subnanoclusters showed characteristic absorption features at 350 nm (3.54 eV) and 375 nm (3.31 eV), without surface plasmon resonance (SPR) in the region between 400 and 450 nm confirming the absence of NPs (Figure 1). To study the effect of temperature

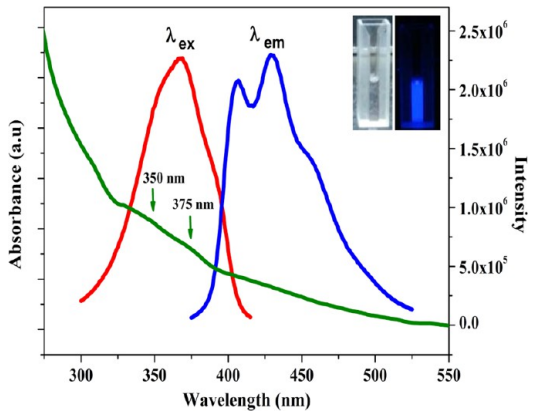

Figure 1. UV−visible (green), fluorescence excitation (red), and emission (blue) spectra of NaC-templated AgNCs. The inset shows photographs of the AgNC solution under visible (left) and UV (right) light.

on the formation AgNCs, the reaction was conducted at 45 °C; the reaction was completed within 35 h, and the obtained products were nanoparticles instead of nanoclusters as evidenced by UV−visible and transmission electron microscopy (TEM) analysis (Figure S1 of the Supporting Information). This shows that the slower reaction is the key requirement for the formation of nanoclusters. Furthermore, with the increase in temperature, the dielectric constant of the medium is significantly lowered, because the repulsive forces between the ionic heads of the molecules increase and the tendency of NaC to associate in the form micelles is weaker,[62] which may lead to destabilization of clusters. Under photoirradiation below and above the CMC, the formed particles were anisotropic (hexagonal/triangular) and spherical in shape, respectively, as evidenced by the HR-TEM images. For spherically shaped particles, the characteristic SPR peak was observed at 408 nm, and for anisotropic particles, a small red shift was observed in the SPR band (Figure S2 of the Supporting Information).

The cluster solution displayed fluorescence with two strong emission maxima and a shoulder at 406, 430, and 456 nm, respectively, with an excitation maximum at 367 nm (Figure 1). The multiple peaks in the emission spectra may be due to the possibility of the existence of small clusters with different association numbers. Similar observations were reported in earlier studies.[12,17,20] To check the fluorescent properties of NaC, we have conducted fluorescence measurements for sodium cholate and compared them with those of NaC-templated AgNCs (Figure S3 of the Supporting Information), which shows that the luminescence is due to only AgNCs and not from the capping agent. In solutions below the CMC, no characteristic emission peak was observed. However, with an increase in the concentration of NaC to a value above CMC, the luminescence intensity of AgNCs significantly increased without any change in the wavelength of emission maxima (Figure 2a). These observations suggest that the formation of

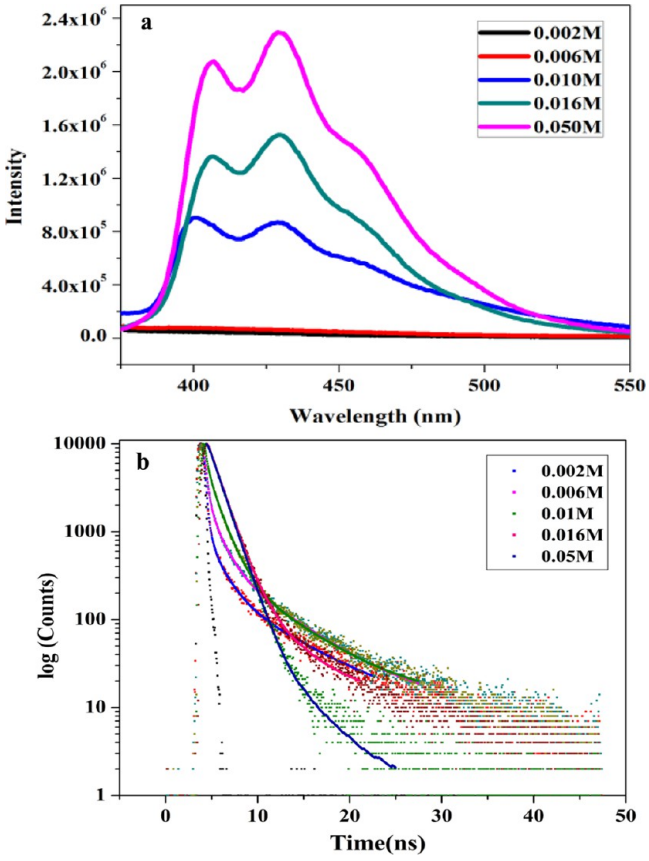

Figure 2. (a) Steady state fluorescence spectra and (b) time-resolved fluorescence lifetime analysis of AgNCs with an increasing NaC concentration.

micelles facilitated more cluster formation without any change in cluster size. A time-dependent steady state fluorescence measurement was performed to evaluate the kinetics of the formation of fluorescent AgNCs in which AgNC samples showed weak fluorescence at the initial stages of the reaction. However, the fluorescence intensity gradually increased with time and eventually reached the saturation level within 4 weeks at room temperature, after which no appreciable change in fluorescence intensity was observed, which in turn confirms the completion of the reaction (Figure S4 of the Supporting Information). The fluorescence quantum yield of the NaC-templated AgNCs was measured to be approximately 20.12% (λ_{ex} = 366 nm) with reference to quinine sulfate (54%) as the standard. To check the stability of AgNCs, changes in the fluorescence intensity were monitored in the absence and presence of UV irradiation. Under dark conditions, no significant change in the fluorescence intensity was noted up

DOI: 10.1021/am507291t
ACS Appl. Mater. Interfaces 2015, 7, 1422−1430

Table 1. Fluorescence Lifetime Data of AgNCs at Various NaC Concentrations at 25 °C (λ_{ex} = 375 nm; λ_{em} = 430 nm)

[NaC] (M)	τ_1 (ns)	α_1 (%)	τ_2 (ns)	α_2 (%)	τ_3 (ns)	α_3 (%)	$\langle\tau\rangle$	χ^2
0.002	0.16	67.85	1.47	15.28	6.50	16.87	1.43	1.10
0.006	0.21	48.63	1.31	27.46	5.76	23.91	1.84	1.09
0.010	0.24	27.08	1.33	55.80	5.77	17.12	1.79	1.12
0.016			1.31	91.04	3.97	08.96	1.55	1.08
0.050			1.35	97.71	4.54	02.29	1.42	1.14

to 40 days, which confirms that the synthesized AgNCs were stable (Figure S5 of the Supporting Information). However, under continuous UV irradiation at 365 nm, the fluorescence intensity started to decrease after 1.5 h and completely disappeared in 6 h (Figure S6 of the Supporting Information). This shows that the minimal time for the UV irradiation-induced transformation of AgNCs into larger nanoparticles is 1.5 h. The fluorescence decays of AgNCs at different NaC concentrations were studied by using a time-correlated single-photon counting (TCSPC) technique (Figure 2b), and the data are listed in Table 1. The vertically polarized 375 nm laser was used to excite the sample. The fluorescence decay profile has been fitted according to eq 2.

$$I(t) = I(0) \sum_{i=1}^{n} \alpha_i \exp(-t/\tau_i) \quad (2)$$

where $I(t)$ is intensity at time t, n is the number of discrete emissive species, and α_i and τ_i are the pre-exponential factor and excited state fluorescence lifetime of the ith component, respectively. In solutions, below and above the CMC, the fluorescence decay of AgNCs was fit with tri- and biexponential functions and the goodness of fit was checked with χ^2 values, which were between 1 and 1.15. At very low NaC concentrations, AgNCs exhibit triexponential behavior (τ_1, τ_2, and τ_3). When the NaC concentration is increased, the relative amplitude of the τ_2 component (α_2) significantly increases whereas the relative amplitudes of the τ_1 and τ_3 components (α_1 and α_3, respectively) gradually decrease. When the concentration of NaC reaches its first CMC, the lower lifetime component τ_1 becomes negligible and the fluorescence decay of AgNCs becomes biexponential. However, in the second CMC, the relative amplitude of the τ_2 component (α_2) increases to a maximum whereas the relative amplitude of the τ_3 component (α_3) decreases to a minimum. The existence of biexponential behavior with lifetimes of 1.35 ns (97.71%) and 4.54 ns (2.29%) could be due to the presence of AgNCs with two different compositions. However, there is no change in the lifetime of the major component with an increase in the NaC concentration, which shows that the size of AgNCs remains unchanged. The existence of tri- and biexponential decays may be due to the difference in polarity around the NaC-templated AgNCs. Above the CMC, AgNCs are embedded in the more hydrophobic region, whereas below the CMC, in addition to the hydrophobic environment, the water molecules also interact with AgNCs; as a result, biexponential becomes triexponential with a low lifetime component (τ_1).

MALDI-TOF MS is a soft ionization technique that allows the determination of cluster composition.[2] The mass spectrum of the synthesized blue light-emitting AgNCs was obtained in positive ion mode using DCTB as a matrix. The MALDI-TOF spectrum showed two peaks at 879.7 and 1131.8 Da for Ag clusters, which are consistent with molecular formulas of $[Ag_4NaC{\cdot}H_2O]^+$ and $[Ag_6NaC{\cdot}3H_2O]^+$, respectively (Figure 3a). Beyond the m/z value of 1200 Da, no peaks were observed. The cluster mass showed that water molecules were also

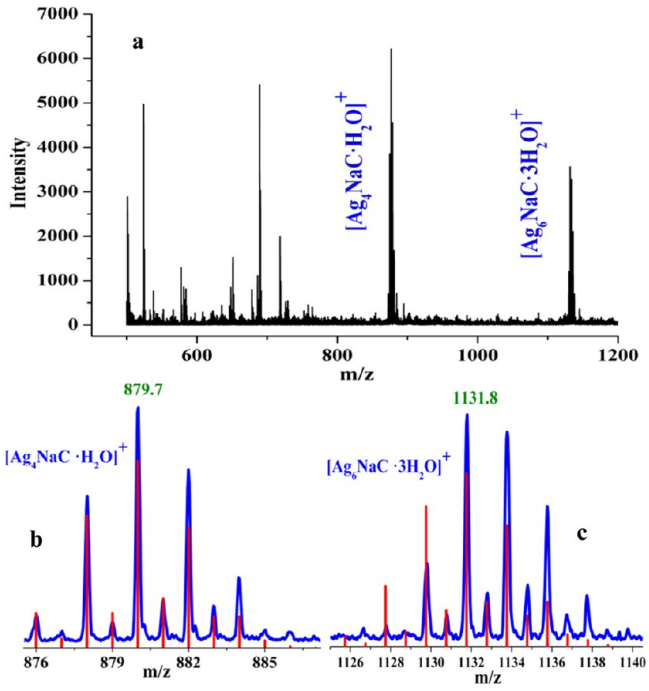

Figure 3. (a) MALDI MS spectrum of NaC-templated AgNCs in positive ion mode and experimental (blue) and simulated (red) isotopic patterns of (b) $[Ag_4NaC{\cdot}H_2O]^+$ and (c) $[Ag_6NaC{\cdot}3H_2O]^+$.

present in the NaC-templated AgNCs because sodium cholate exists as a hydrate. Dickson et al. have also reported the presence of water molecules in the PAMAM dendrimer-templated Au_8 nanocluster using ESI MS.[63] The experimentally observed isotope distribution matched perfectly with the simulated pattern (Figure 3b,c). The well-defined isotope patterns with a separation of m/z 2 revealed that the overall species was singly charged. On the basis of the MALDI-TOF MS analysis, we can conclude that the clusters are mainly composed of four and six Ag atoms. We also performed electrospray ionization mass spectroscopy (ESI MS) measurements for the synthesized AgNCs in positive ion mode (Figure S7 of the Supporting Information), which is consistent with the MALDI-TOF MS results.

HR-TEM was used to confirm the size of AgNCs and AgNPs. The TEM images of the cluster (Figure 4a–f) showed that the clusters were nearly monodisperse with an average size of 0.4 ± 0.2 nm and larger Ag particles were not detected, showing that the method used in this study is very efficient in producing Ag subnanoclusters. Under photoirradiation above the CMC, spherically shaped NPs were formed in 5 h with an average size of 7 ± 0.5 nm; after irradiation for 7 h, the size of the particles was found to be 8 ± 0.5 nm without any changes

DOI: 10.1021/am507291t
ACS Appl. Mater. Interfaces 2015, 7, 1422–1430

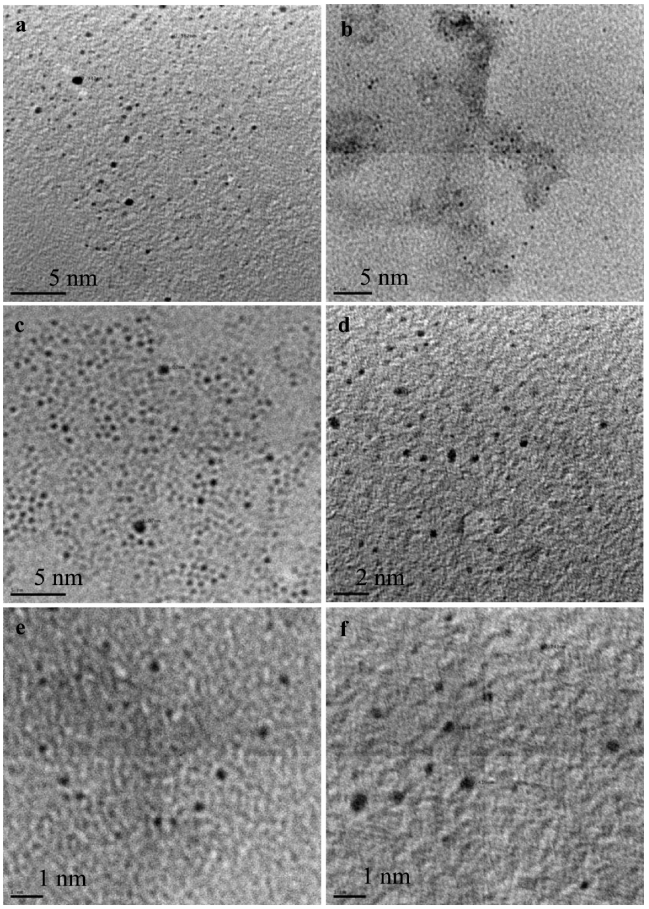

Figure 4. TEM images of NaC-templated AgNCs at different magnifications.

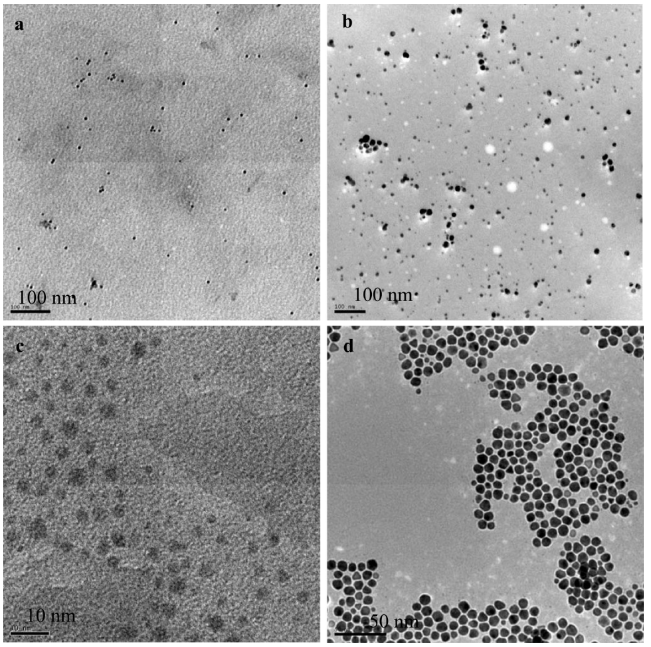

Figure 5. TEM images of as-synthesized AgNPs above the CMC of NaC (0.05 M) under UV irradiation at 365 nm for (a) 5 h and (b) 7 h. TEM images of as-synthesized AgNPs below the CMC of NaC (0.015 M) under UV irradiation at 365 nm for (c) 5 h and (d) 7 h.

in shape (Figure 5a,b). However, below the CMC after irradiation for 5 h, small spherically shaped NPs (average size of 4 ± 0.3 nm) were formed, and when the irradiation time was increased to 7 h, the obtained particles were found to be anisotropic in nature (hexagonal/triangular) with an average size of 9 ± 0.5 nm (Figure 5c,d) because, above the CMC, the formed particles are effectively stabilized by the carboxylate groups that are present on the surface of the micelles. However, below the CMC, the initially formed small spherically shaped particles do not effectively engage in capping the particles, so that light-induced hexagonal and triangular particle formation becomes possible.

The involvement of -OH groups for the reduction of Ag^+ ions was further confirmed by FT-IR analysis (Figure S8 of the Supporting Information). The shift toward a lower frequency (1555 cm^{-1}) by the NaC-capped AgNPs in comparison to the asymmetric stretching band observed at 1580 cm^{-1} by the COO^- group in pure NaC indicates the role of the COO^- group as a capping ligand for the stabilization of AgNPs. Further, new bands appeared around 1713 and 1750 cm^{-1} (marked by the circle) and could be due to the presence of keto carbonyl groups, which indicates the oxidation of OH groups for the reduction of metal ions. The XPS survey spectrum shows all the expected elements (Ag, C, and O). The high-resolution spectrum of silver shows Ag in the Ag(0) state (Figure S9 of the Supporting Information). The $3d_{5/2}$ core level binding energy was observed at 368.35 eV for AgNCs. A small shift toward a higher binding energy is due to the ultrasmall cluster size.

Further, to study stability in organic solvents, the synthesized clusters were ligand exchanged using phenylethanethiol (PET) and transferred to the toluene medium. The exchanged clusters show absorption features at 350 and 375 nm that match the absorption features of the NaC-templated AgNCs. Fluorescence spectra of ligand-exchanged clusters show two strong emission maxima and a shoulder at 406, 430, and 456 nm, respectively, with an excitation maximum at 367 nm that also perfectly matches the emission spectra of NaC-capped AgNCs, which proves that the cluster core remains unaffected even after ligand exchange (Figure 6).

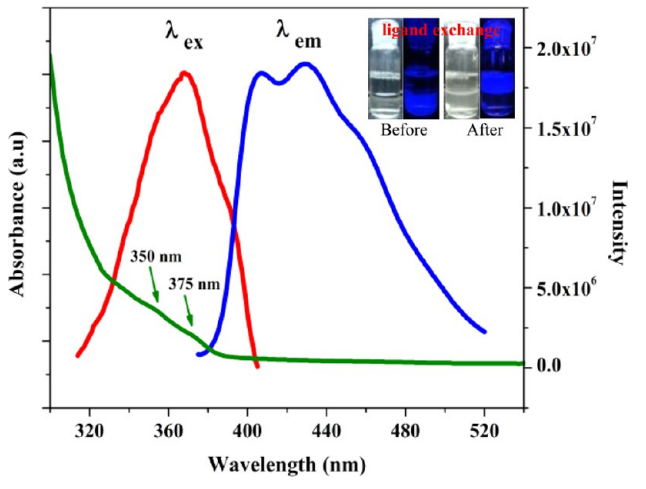

Figure 6. UV−visible (green), fluorescence excitation (red), and emission (blue) spectra of PET-exchanged AgNCs in toluene. The inset shows photographs of the AgNC solution before and after ligand exchange under visible and UV light (365 nm).

DOI: 10.1021/am507291t
ACS Appl. Mater. Interfaces 2015, 7, 1422−1430

Toxicity and Bioimaging Studies of AgNCs in Zebrafish Embryos. To evaluate the effect of AgNCs on the embryonic development of zebrafish, we exposed the embryos to different concentrations of AgNCs (25, 50, 100, and 200 μL/mL) for 4−96 hpf and directly observed the toxicity at different stages using an inverted microscope. In the survival experiment, none of the embryos became deformed and a majority of the embryos developed normally into zebrafish, which shows that no significant adverse effect was observed up to 200 μL/mL AgNCs (Figure 7a). In the hatching experiment, larvae began

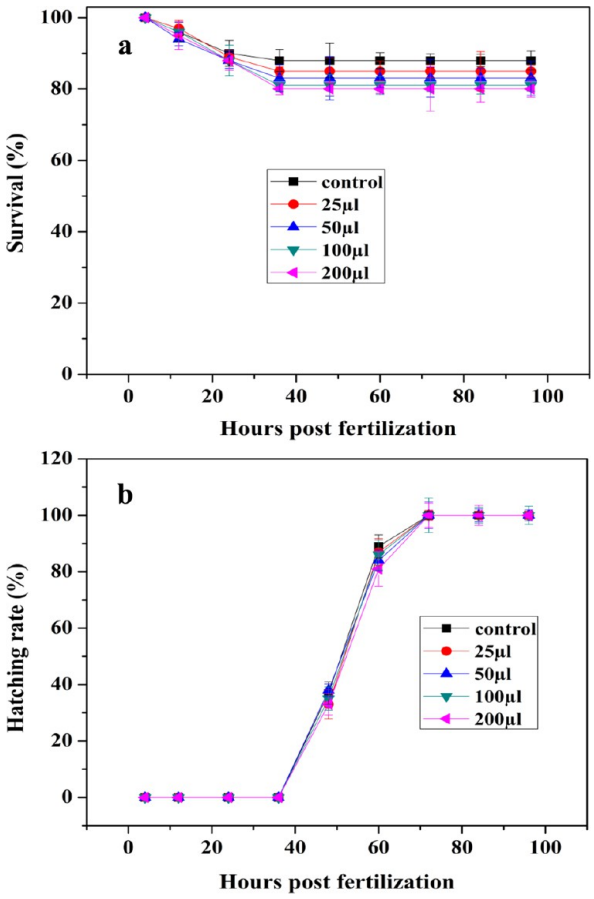

Figure 7. (a) Survival and (b) hatching experiments with zebrafish embryos exposed to different concentrations of AgNCs over 96 hpf. No statistically significant effects occurred between control and AgNC-exposed embryos (N = 100 or 20 embryos; five replicates each).

to hatch between 48 and 72 hpf, which is the normal hatching period of zebrafish embryos (Figure 7b). Furthermore, the AgNC-stained embryos imaged at late gastrula stage (10 hpf), pharyngula stage (24 hpf), hatching stage (48 hpf), and larval stage (96 hpf) with a fluorescence microscope using a blue filter show blue luminescence at the inner membrane of the embryos (Figure 8), and the intensity of the fluorescence increases as the AgNC concentration increases to 200 μL/mL. The observed blue fluorescence at the inner membrane of embryos could be due to the passive diffusion of ultrasmall AgNCs through chorion canals of embryo and stays inside the embryos throughout embryonic development (96 hpf). The intensity of the fluorescence remains the same over the period from 4 to 96 hpf in zebrafish embryos, which shows that AgNCs are more stable in living systems. These finding indicates that the AgNCs are nontoxic, exhibit bright fluorescence, and are stable in

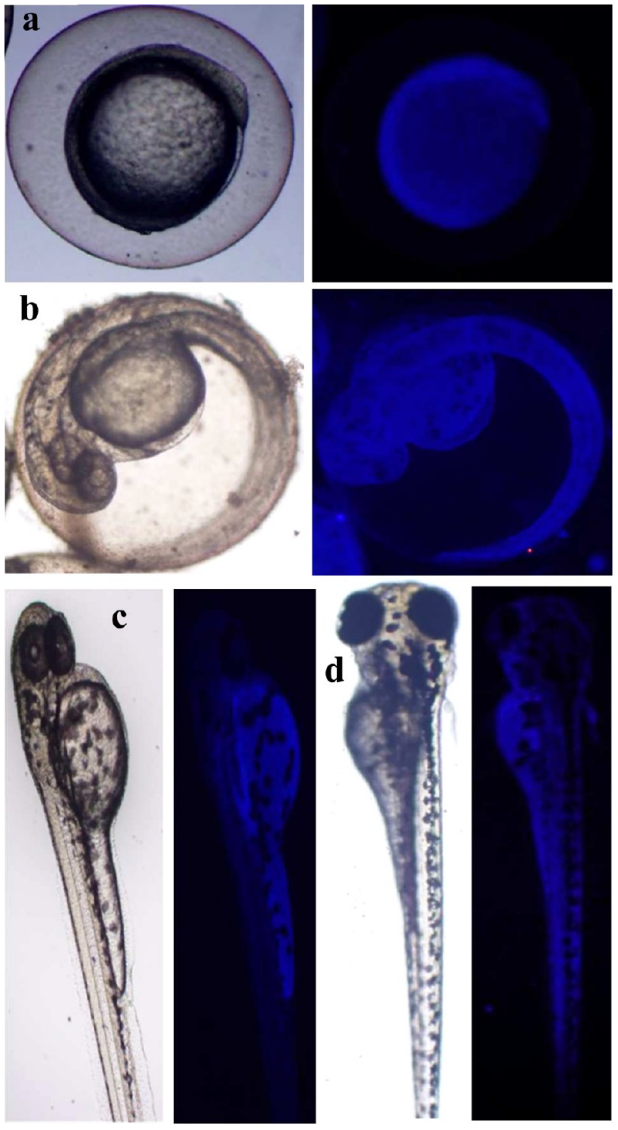

Figure 8. Bright-field (left) and fluorescent images (right) of zebrafish embryos at different stages exposed to 200 μL/mL AgNCs: (a) late gastrula stage (10 hpf), (b) pharyngula stage (24 hpf), (c) hatching stage (48 hpf), and (d) larval stage (96 hpf).

biological media, which could be used as an effective fluorescent probe for *in vivo* bioimaging applications.

CONCLUSION

In conclusion, water-soluble, highly stable, blue light-emitting Ag subnanoclusters have been successfully synthesized by a simple approach using NaC as the template above the CMC at room temperature. In addition, under UV light irradiation below and above the CMC, small anisotropic and spherically shaped 3−11 nm NPs were prepared. The synthesized Ag nanoclusters with an average size of 0.4 ± 0.2 nm possess four- and six-Ag atom cores with well-defined excitation and emission spectra. The clusters were characterized by UV−visible, HR-TEM, FT-IR, spectrofluorimeter, TCSPC, XPS, and MALDI-TOF MS. These clusters were phase transferred from aqueous to organic medium by ligand exchange using PET, and the exchanged clusters retained all the distinct optical features. Also, we conducted toxicity and bioimaging studies of NaC-templated AgNCs using zebrafish embryos as an *in vivo* model,

DOI: 10.1021/am507291t
ACS Appl. Mater. Interfaces 2015, 7, 1422−1430

which shows that the synthesized AgNCs have very low toxic and are highly fluorescent in zebrafish embryos. The protocol developed in this study provides an efficient and "green" approach for the production of ultrafine sized, highly luminescent, and biocompatible AgNCs that could be used as potential fluorescent probes for both *in vitro* and *in vivo* bioimaging applications.

■ ASSOCIATED CONTENT

Supporting Information

UV−visible, FT-IR, and XPS data. This material is available free of charge via the Internet at http://pubs.acs.org.

■ AUTHOR INFORMATION

Corresponding Author

*E-mail: nrajendiar@yahoo.com.

Notes

The authors declare no competing financial interest.

■ ACKNOWLEDGMENTS

We thank the Department of Science and Technology (SR/FT/CS-089/2009), Government of India, for financial support. The National Centre for Nanoscience and Nanotechnology, University of Madras, is thanked for the HR-TEM and XPS analysis. The National Centre for Ultrafast Processes, University of Madras, is thanked for the lifetime measurements. The DST unit of Nanoscience, IIT Madras, is thanked for the MALDI-TOF MS analysis. We thank Dr. Suvro Chatterjee (AU-KBC Research Centre, Life Sciences, MIT Campus, Anna University) for providing the fluorescence microscope facility.

■ REFERENCES

(1) Zheng, J.; Nicovich, P. R.; Dickson, R. M. Highly Fluorescent Noble-Metal Quantum Dots. *Annu. Rev. Phys. Chem.* **2007**, *58*, 409−431.

(2) Lu, Y.; Chen, W. Sub-Nanometre Sized Metal Clusters: From Synthetic Challenges to the Unique Property Discoveries. *Chem. Soc. Rev.* **2012**, *41*, 3594−3623.

(3) Rao, T. U. B.; Nataraju, B.; Pradeep, T. Ag_9 Quantum Cluster through a Solid-State Route. *J. Am. Chem. Soc.* **2010**, *132*, 16304−16307.

(4) Ledo-Suarez, A.; Rivas, J.; Rodriguez-Abreu, C. F.; Rodriguez, M. J.; Pastor, E.; Hernandez-Creus, A.; Oseroff, S. B.; Lopez-Quintela, M. A. Facile Synthesis of Stable Subnanosized Silver Clusters in Microemulsions. *Angew. Chem., Int. Ed.* **2007**, *46*, 8823−8827.

(5) Richards, C. I.; Choi, S.; Hsiang, J. C.; Antoku, Y.; Vosch, T.; Bongiorno, A.; Tzeng, Y. L.; Dickson, R. M. Oligonucleotide-Stabilized Ag Nanocluster Fluorophores. *J. Am. Chem. Soc.* **2008**, *130*, 5038−5039.

(6) Chen, W. Y.; Lan, G. Y.; Chang, H. T. Use of Fluorescent DNA-Templated Gold/Silver Nanoclusters for the Detection of Sulfide Ions. *Anal. Chem.* **2011**, *83*, 9450−9455.

(7) Liu, S.; Lu, F.; Zhu, J. J. Highly Fluorescent Ag Nanoclusters: Microwave-Assisted Green Synthesis and Cr^{3+} Sensing. *Chem. Commun.* **2011**, *47*, 2661−2663.

(8) Choi, S.; Dickson, R. M.; Yu, J. Developing Luminescent Silver Nanodots for Biological Applications. *Chem. Soc. Rev.* **2012**, *41*, 1867−1891.

(9) Lei, Y.; Mehmood, F.; Lee, S.; Greeley, J.; Lee, B.; Seifert, S.; Winans, R. E.; Elam, J. W.; Meyer, R. J.; Redfern, P. C.; Teschner, D.; Schlögl, R.; Pellin, M. J.; Curtiss, L. A.; Vajda, S. Increased Silver Activity for Direct Propylene Epoxidation via Subnanometer Size Effects. *Science* **2010**, *328*, 224−228.

(10) Lin, C. A. J.; Yang, T. Y.; Lee, C. H.; Huang, S. H.; Sperling, R. A.; Zanella, M.; Li, J. K.; Shen, J. L.; Wang, H. H.; Yeh, H. I.; Parak, W. J.; Chang, W. H. Synthesis, Characterization, and Bioconjugation of Fluorescent Gold Nanoclusters toward Biological Labeling Applications. *ACS Nano* **2009**, *3*, 395−401.

(11) Jin, R. Quantum Sized, Thiolate-Protected Gold Nanoclusters. *Nanoscale* **2010**, *2*, 343−362.

(12) Petty, J. T.; Zheng, J.; Hud, N. V.; Dickson, R. M. DNA-Templated Ag Nanocluster Formation. *J. Am. Chem. Soc.* **2004**, *126*, 5207−5212.

(13) Sharma, J.; Yeh, H. C.; Yoo, H.; Werner, J. H.; Martinez, J. S. A Complementary Palette of Fluorescent Silver Nanoclusters. *Chem. Commun.* **2010**, *46*, 3280−3282.

(14) Koszinowski, K.; Ballweg, K. A Highly Charged Ag_6^{4+} Core in a DNA-Encapsulated Silver Nanocluster. *Chem.—Eur. J.* **2010**, *16*, 3285−3290.

(15) Guo, W.; Yuan, J.; Dong, Q.; Wang, E. Highly Sequence-Dependent Formation of Fluorescent Silver Nanoclusters in Hybridized DNA Duplexes for Single Nucleotide Mutation Identification. *J. Am. Chem. Soc.* **2010**, *132*, 932−934.

(16) Yang, X.; Gan, L.; Han, L.; Wang, E.; Wang, J. High-Yield Synthesis of Silver Nanoclusters Protected by DNA Monomers and DFT Prediction of their Photoluminescence Properties. *Angew. Chem., Int. Ed.* **2013**, *52*, 2022−2026.

(17) Cui, Y.; Wang, Y.; Liu, R.; Sun, Z.; Wei, Y.; Zhao, Y.; Gao, X. Serial Silver Clusters Biomineralized by One Peptide. *ACS Nano* **2011**, *5*, 8684−8689.

(18) Anand, U.; Ghosh, S.; Mukherjee, S. Toggling Between Blue and Red-Emitting Fluorescent Silver Nanoclusters. *J. Phys. Chem. Lett.* **2012**, *3*, 3605−3609.

(19) Zhang, J.; Xu, S.; Kumacheva, E. Photogeneration of Fluorescent Silver Nanoclusters in Polymer Microgels. *Adv. Mater.* **2005**, *17*, 2336−2340.

(20) Shen, Z.; Duan, H.; Frey, H. Water-Soluble Fluorescent Ag Nanoclusters Obtained from Multiarm Star Poly(acrylic acid) as "Molecular Hydrogel" Templates. *Adv. Mater.* **2007**, *19*, 349−352.

(21) Shang, L.; Dong, S. Facile Preparation of Water-Soluble Fluorescent Silver Nanoclusters Using a Polyelectrolyte Template. *Chem. Commun.* **2008**, 1088−1090.

(22) Diez, I.; Pusa, M.; Kulmala, S.; Jiang, H.; Walther, A.; Goldmann, A. S.; Muller, A. H. E.; Ikkala, O.; Ras, R. H. A. Color Tunability and Electrochemiluminescence of Silver Nanoclusters. *Angew. Chem., Int. Ed.* **2009**, *48*, 2122−2125.

(23) Xu, H.; Suslick, K. S. Sonochemical Synthesis of Highly Fluorescent Ag Nanoclusters. *ACS Nano* **2010**, *4*, 3209−3214.

(24) Qu, F.; Dou, L. L.; Li, N. B.; Luo, H. Q. Solvatofluorochromism of Polyethyleneimine-Encapsulated Ag Nanoclusters and their Concentration-Dependent Fluorescence. *J. Mater. Chem. C* **2013**, *1*, 4008−4013.

(25) Li, Y.; Wang, X.; Xu, S.; Xu, W. The Solvent Effect on the Luminescence of Silver Nanoclusters. *Phys. Chem. Chem. Phys.* **2013**, *15*, 2665−2668.

(26) Zheng, J.; Dickson, R. M. Communication Individual Water-Soluble Dendrimer-Encapsulated Silver Nanodot Fluorescence. *J. Am. Chem. Soc.* **2002**, *124*, 13982−13983.

(27) Kumar, S.; Bolan, M. D.; Bigioni, T. P. Glutathione-Stabilized Magic-Number Silver Cluster Compounds. *J. Am. Chem. Soc.* **2010**, *132*, 13141−13143.

(28) Adhikari, B.; Banerjee, A. Facile Synthesis of Water-Soluble Fluorescent Silver Nanoclusters and Hg^{II} Sensing. *Chem. Mater.* **2010**, *22*, 4364−4371.

(29) Rao, T. U. B.; Pradeep, T. Luminescent Ag_7 and Ag_8 Clusters by Interfacial Synthesis. *Angew. Chem., Int. Ed.* **2010**, *49*, 3925−3929.

(30) Wu, Z.; Lanni, E.; Chen, W.; Bier, M. E.; Ly, D.; Jin, R. High Yield, Large Scale Synthesis of Thiolate-Protected Ag_7 Clusters. *J. Am. Chem. Soc.* **2009**, *131*, 16672−16674.

(31) Huang, S.; Pfeiffer, C.; Hollmann, J.; Friede, S.; Jin-Ching Chen, J.; Beyer, A.; Haas, B.; Volz, K.; Heimbrodt, W.; Martos, J. M. M.; Chang, W.; Parak, W. J. Synthesis and Characterization of Colloidal Fluorescent Silver Nanoclusters. *Langmuir* **2012**, *28*, 8915−8919.

DOI: 10.1021/am507291t
ACS Appl. Mater. Interfaces 2015, 7, 1422−1430

(32) Yuan, X.; Luo, Z.; Zhang, Q.; Zhang, X.; Zheng, Y.; Lee, J. Y.; Xie, J. Synthesis of Highly Fluorescent Metal (Ag, Au, Pt, and Cu) Nanoclusters by Electrostatically Induced Reversible Phase Transfer. *ACS Nano* **2011**, *5*, 8800−8808.
(33) Yang, H.; Lei, J.; Wu, B.; Wang, Y.; Zhou, M.; Xia, A.; Zhenga, L.; Zheng, N. Crystal Structure of a Luminescent Thiolated Ag Nanocluster with an Octahedral Ag_6^{4+} Core. *Chem. Commun.* **2013**, *49*, 300−302.
(34) Muhammed, M. A. H.; Aldeek, F.; Palui, G.; Trapiella-Alfonso, L.; Mattoussi, H. Growth of *In Situ* Functionalized Luminescent Silver Nanoclusters by Direct Reduction and Size Focusing. *ACS Nano* **2012**, *6*, 8950−8961.
(35) Roy, S.; Baral, A.; Banerjee, A. Tuning of Silver Cluster Emission from Blue to Red Using a Bio-Active Peptide in Water. *ACS Appl. Mater. Interfaces* **2014**, *6*, 4050−4056.
(36) Adhikari, B.; Banerjee, A. Short-Peptide-Based Hydrogel: A Template for the In Situ Synthesis of Fluorescent Silver Nanoclusters by Using Sunlight. *Chem.—Eur. J.* **2010**, *16*, 13698−13705.
(37) Roy, S.; Banerjee, A. Amino Acid Based Smart Hydrogel: Formation, Characterization and Fluorescence Properties of Silver Nanoclusters within the Hydrogel Matrix. *Soft Matter* **2011**, *7*, 5300−5308.
(38) Huang, X.; Li, B.; Li, L.; Zhang, H.; Majeed, I.; Hussain, I.; Tan, B. Facile Preparation of Highly Blue Fluorescent Metal Nanoclusters in Organic Media. *J. Phys. Chem. C* **2012**, *116*, 448−455.
(39) Zhou, T.; Rong, M.; Cai, Z.; Yang, C. J.; Chen, X. Sonochemical Synthesis of Highly Fluorescent Glutathione-Stabilized Ag Nanoclusters and S^{2-} Sensing. *Nanoscale* **2012**, *4*, 4103−4106.
(40) Small, D. M. (1971) The Physical Chemistry of Cholanic Acids. In *The Bile Acids* (Nair, P. P., and Kritchevsky, D., Eds.) Vol. *1*, pp 249−356, Plenum Publishing Corp., New York.
(41) Wu, X.; He, X.; Wang, K.; Xie, C.; Zhou, B.; Qing, Z. Ultrasmall Near-Infrared Gold Nanoclusters for Tumor Fluorescence Imaging *In Vivo*. *Nanoscale* **2010**, *2*, 2244−2249.
(42) Wang, J.; Zhang, G.; Li, Q.; Jiang, H.; Liu, C.; Amatore, C.; Wang, X. *In Vivo* Self-Bio-Imaging of Tumors through *In Situ* Biosynthesized Fluorescent Gold Nanoclusters. *Sci. Rep.* **2013**, *3*, 1157.
(43) Gao, S.; Chen, D.; Li, Q.; Ye, J.; Jiang, H.; Amatore, C.; Wang, X. Near-Infrared Fluorescence Imaging of Cancer Cells and Tumors through Specific Biosynthesis of Silver Nanoclusters. *Sci. Rep.* **2014**, *4*, 4384.
(44) Wang, H. H.; Lin, C. A. J.; Lee, C. H.; Lin, Y. C.; Tseng, Y. M.; Hsieh, C. L.; Chen, C. H.; Tsai, C. H.; Hsieh, C. T.; Shen, J. L.; Chan, W. H.; Chang, W. H.; Yeh, H. I. Fluorescent Gold Nanoclusters as a Biocompatible Marker for *In Vitro* and *In Vivo* Tracking of Endothelial Cells. *ACS Nano* **2011**, *5*, 4337−4344.
(45) Zhang, P.; Yang, X. X.; Wang, Y.; Zhao, N. W.; Xiong, Z. H.; Huang, C. Z. Rapid Synthesis of Highly Luminescent and Stable Au_{20} Nanoclusters for Active Tumor-Targeted Imaging *In Vitro* and *In Vivo*. *Nanoscale* **2014**, *6*, 2261−2269.
(46) Fako, V. E.; Furgeson, D. Y. Zebrafish as a Correlative and Predictive Model for Assessing Biomaterial Nanotoxicity. *Adv. Drug Delivery Rev.* **2009**, *61*, 478−486.
(47) Alsop, D.; Wood, C. M. Metal Uptake and Acute Toxicity in Zebrafish: Common Mechanisms Across Multiple Metals. *Aquat. Toxicol.* **2011**, *105*, 385−393.
(48) Kwon, N. Y.; Kim, D.; Jang, G.; Lee, J. H.; So, J. H.; Kim, C. H.; Kim, T. H.; Lee, T. S. Highly Selective Cysteine Detection and Bioimaging in Zebrafish through Emission Color Change of Water-Soluble Conjugated Polymer-Based Assay Complex. *ACS Appl. Mater. Interfaces* **2012**, *4*, 1429−1433.
(49) Basu, S.; Sachidanandan, C. Zebrafish: A Multifaceted Tool for Chemical Biologists. *Chem. Rev.* **2013**, *113*, 7952−7980.
(50) Fent, K.; Weisbrod, C. J.; Heller, A. W.; Pieles, U. Assessment of Uptake and Toxicity of Fluorescent Silica Nanoparticles in Zebrafish (*Danio rerio*) Early Life Stages. *Aquat. Toxicol.* **2010**, *100*, 218−228.
(51) Duan, J.; Yu, Y.; Li, Y.; Yu, Y.; Sun, Z. Cardiovascular Toxicity Evaluation of Silica Nanoparticles in Endothelial Cells and Zebrafish Model. *Biomaterials* **2013**, *34*, 5853−5862.
(52) Lin, S.; Zhao, Y.; Xia, T.; Meng, H.; Ji, Z.; Liu, R.; George, S.; Xiong, S.; Wang, X.; Zhang, H.; Pokhrel, S.; Madler, L.; Damoiseaux, R.; Lin, S.; Nel, A. E. High Content Screening in Zebrafish Speeds up Hazard Ranking of Transition Metal Oxide Nanoparticles. *ACS Nano* **2011**, *5*, 7284−7295.
(53) Wang, Y.; Seebald, J. L.; Szeto, D. P.; Irudayaraj, J. Biocompatibility and Biodistribution of Surface-Enhanced Raman Scattering Nanoprobes in Zebrafish Embryos: *In Vivo* and Multiplex Imaging. *ACS Nano* **2010**, *4*, 4039−4053.
(54) Harper, S. L.; Carriere, J. L.; Miller, J. M.; Hutchison, J. E.; Maddux, B. L. S.; Tanguay, R. L. Systematic Evaluation of Nanomaterial Toxicity: Utility of Standardized Materials and Rapid Assays. *ACS Nano* **2011**, *5*, 4688−4697.
(55) Lee, K. J.; Nallathamby, P. D.; Browning, L. M.; Osgood, C. J.; Xu, X. H. N. *In Vivo* Imaging of Transport and Biocompatibility of Single Silver Nanoparticles in Early Development of Zebrafish Embryos. *ACS Nano* **2007**, *1*, 133−143.
(56) George, S.; Xia, T.; Rallo, R.; Zhao, Y.; Ji, Z.; Lin, S.; Wang, X.; Zhang, H.; France, B.; Schoenfeld, D.; Damoiseaux, R.; Liu, R.; Lin, S.; Bradley, K. A.; Cohen, Y.; Nel, A. E. Use of a High-Throughput Screening Approach Coupled with *In Vivo* Zebrafish Embryo Screening to Develop Hazard Ranking for Engineered Nanomaterials. *ACS Nano* **2011**, *5*, 1805−1817.
(57) Kim, M. S.; Louis, K. M.; Pedersen, J. A.; Hamers, R. J.; Peterson, R. E.; Heideman, W. Using Citrate-Functionalized TiO_2 Nanoparticles to Study the Effect of Particle Size on Zebrafish Embryo Toxicity. *Analyst* **2014**, *139*, 964−992.
(58) Ko, S. K.; Chen, X.; Yoon, J.; Shin, I. Zebrafish as a Good Vertebrate Model for Molecular Imaging using Fluorescent Probes. *Chem. Soc. Rev.* **2011**, *40*, 2120−2130.
(59) Yang, Y. K.; Cho, H. J.; Lee, J.; Shin, I.; Tae, J. A Rhodamine-Hydroxamic Acid-Based Fluorescent Probe for Hypochlorous Acid and Its Applications to Biological Imagings. *Org. Lett.* **2009**, *11*, 859−861.
(60) Meyerhoffer, S. M.; McGown, L. B. Microenvironments of Fluorescence Probes in Sodium Taurocholate and Sodium Taurodeoxycholate Bile Salt Media. *Anal. Chem.* **1991**, *63*, 2082−2086.
(61) Zana, R.; Guveli, D. Fluorescence Probing Study of the Association of Brie Salts in Aqueous Solutions. *J. Phys. Chem.* **1985**, *89*, 1687−1690.
(62) Carey, M. C.; Small, D. M. Micellar Properties of Dihydroxy and Trihydroxy Bile Salts: Effects of Counterion and Temperature. *J. Colloid Interface Sci.* **1969**, *31*, 382−396.
(63) Zheng, J.; Petty, J. T.; Dickson, R. M. High Quantum Yield Blue Emission from Water-Soluble Au_8 Nanodots. *J. Am. Chem. Soc.* **2003**, *125*, 7780−7781.

DOI: 10.1021/am507291t
ACS Appl. Mater. Interfaces 2015, 7, 1422−1430